CHEMISTRY OF MATERIALS
Cite This: Chem. Mater. 2018, 30, 8732–8738
Article
pubs.acs.org/cm

Quantifying the Exfoliation Ease Level of 2D Materials via Mechanical Anisotropy

Li-Jun Ji,[†] Yan Qin,[†] Di Gui,[†] Wei Li,*[,†,∥] Yanchun Li,[‡] Xiaodong Li,[‡] and Peixiang Lu*[,†,§]

[†]School of Physics and Wuhan National Laboratory for Optoelectronics, Huazhong University of Science and Technology, Wuhan 430074, China

[‡]Beijing Synchrotron Radiation Facility, Institute of High Energy Physics, Chinese Academy of Sciences, Beijing 100049, China

[§]Laboratory for Optical Information Technology, Wuhan Institute of Technology, Wuhan 430205, China

[∥]School of Materials Science and Engineering & National Institute for Advanced Materials, Nankai University, Tianjin 300350, China

Supporting Information

ABSTRACT: The isolation of 2D materials from mother bulks into nanoscale is of vital importance for fulfilling their applications in many technological fields. Among known methods, mechanical exfoliation is one of the most widely utilized ways due to its simplicity. For a given 2D material, both its interlayer and its intralayer bonding strengths need to be taken into account for understanding the exfoliation process as the former dominates the ease level for cleaving adjacent molecular layers while the latter regulates the ability to resist cracking. In this regard, strong intralayer but weak interlayer bonding interactions respectively lead to large and thin nanosheets and, hence, facile exfoliation (and vice versa). As the bonding forces can be directly reflected through elastic properties of materials, here we propose to use the ratio between the in-plane and out-of-plane elastic modulus (E) as a universal index, $A_{In/Out}$ ($= E_{In\text{-}plane}/E_{Out\text{-}of\text{-}plane}$), to quantify the ease level of a 2D material's mechanical exfoliation. Such ratios, which can be facilely obtained from routine computational and mechanical experiments, could provide useful information for estimating suitable exfoliation methods of 2D materials.

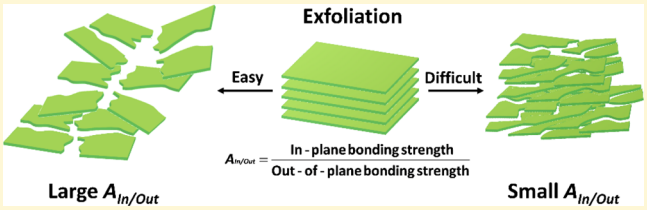

INTRODUCTION

2D materials are a diverse family of materials which show exotic physical properties in the nanoscale endowed by their intrinsic quantum confinement nature.[1,2] To fulfill their application potentials, they need to be thinned into nanosheets. Hitherto, various preparation methods have been developed to obtain ultrathin nanosheets,[3−6] and mechanical exfoliation is one of the most widely used methods due to its simplicity.[7] For some 2D materials, in which the interlayers interact via weak van der Waals forces, such as graphite[1] and MoS_2,[8] the facile mechanical cleavage method (i.e., Scotch taping) has been broadly utilized to peel off mono- and multilayers from their mother bulks. Considering some densely stacked 2D metal−organic frameworks (MOFs)[9] and layered double hydroxides (LDHs),[10] in which the adjacent layers are bound via stronger molecular interactions (i.e., H-bonding, electrostatic forces), more violent exfoliating methods, such as the liquid phase exfoliation,[7] are required for splitting bulk solids into the thin nanosheets. Clearly, the difficulty level of exfoliation depends on the specific structure of a given 2D material and corresponding contrast between the strong in-plane bonding and weak out-of-plane interactions. In this regard, a 2D material's mechanical anisotropy needs to be well understood as it provides critical information for choosing suitable exfoliation routes, particularly considering the increasing demand for scaling down many newly emerged 2D bulk materials into thin nanosheets. However, little attention has been paid to the thorough understanding of this important field, and the exfoliation ease level of 2D materials is still disconnected from their molecular mechanics. Here, we systematically investigate the physical exfoliation of eight prototypical 2D materials with diverse molecular bonding forces at same experimental conditions. Our statistical TEM and AFM analyses demonstrate that the exfoliated nanosheets of each 2D material show distinct thickness and lateral dimensions depending on its in-plane and out-of-plane bonding strengths. We reveal the ease levels for exfoliating these 2D materials into thin nanosheets are proportional to the magnitude of their mechanical anisotropies between in-plane and out-of-plane.

RESULTS AND DISCUSSION

We selected eight representative 2D materials with diverse inter- and intralayer bonding interactions for the study. In graphite, h-BN, MoS_2, WS_2, black phosphorus, and metal−organic framework $Mn(C_6H_8O_4)(H_2O)$[11] (Figure 1a−f), their

Received: March 13, 2018
Revised: November 23, 2018
Published: November 26, 2018

DOI: 10.1021/acs.chemmater.8b01082
Chem. Mater. 2018, 30, 8732−8738

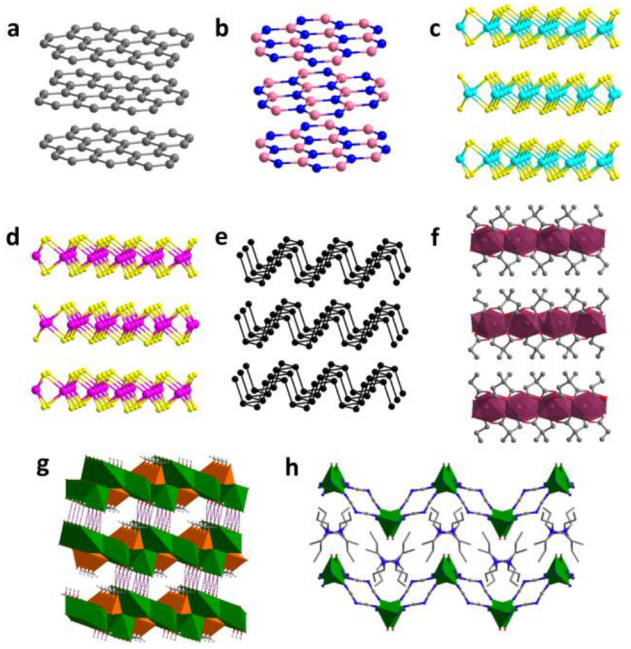

Figure 1. Crystal structures of eight prototypical 2D materials. (a) Graphite, (b) *h*-BN, (c) MoS_2, (d) WS_2, (e) black phosphorus (black P), (f) $Mn(C_6H_8O_4)(H_2O)$ (MnDMS), (g) $Cu_{1.5}(H_2O)[O_3PCH_2CO_2]$ (Cu-P), and (h) $(TPrA)Cu(NO_3)(dca)_2$ (Cu-dca). Color scheme: C, dark gray; H, light gray; O, red; N, blue; B, pink; Mo, turquoise; S, yellow; W, magenta; black P, black; Mn, plum; Cu^{2+}, olive; P^{3+}, orange. The nitrate groups and the hydrogen atoms of $(TPrA)^+$ cations and $Mn(C_6H_8O_4)(H_2O)$ are omitted for clarity.

intralayer atoms are bound via strong covalent or coordination bonds while adjacent layers are interacted via much weaker van der Waals forces. It is well-known that these six 2D materials can be easily exfoliated into mono- or few-layers nanosheets with large lateral sizes by facile mechanical exfoliation (i.e., Scotch taping, moderate liquid sonication). We also chose a layered coordination polymer (CP) $Cu_{1.5}(H_2O)[O_3PCH_2CO_2]$[9] in which the neighboring wrinkled coordination layers are tied via H-bonding (Figure 1g). In addition, we synthesized a new 2D coordination polymer $(TPrA)Cu(NO_3)(dca)_2$ in which the anionic $[Cu(NO_3)(dca)_2]^-$ layers are charge balanced by the homogeneously dispersed dendrimetric $TPrA^+$ guest cations in the gaps between adjacent layers (Figure 1h).

To examine the liquid-assisted exfoliation of these eight 2D materials at the same conditions, we dispersed 1 mg of crystals of each material in 1 mL of ethanol and sonicated for 30 min. The obtained colloidal suspensions show obvious Tyndall effect under laser beam, which suggests the effective exfoliation. To obtain direct evidence of the successful exfoliation, transmission electron microscopy (TEM) characterizations were performed to examine the morphology and crystallinity of the obtained nanosheets. As presented in the bright field images in Figure 2, the flakes lie flat on the copper mesh with various shapes and diverse ranges of lateral sizes. The dark and bright areas correspond to thicker and thinner nanosheets, respectively. The overlap of these nanosheets possibly arises from the incomplete cleavage and restacking due to the interlayer interactions.[12,13] From bright field images in Figure 2, the average length ($\langle L \rangle$) of graphite nanosheets is about 243.5 nm (Figure 2q), and the peak calculated by the log-normal[14−16] fitting of the distribution is about 169 ± 4 nm, indicating the most probable length (L) of the exfoliated nanosheets. The high resolution TEM (HRTEM) image shows lattice fringes of about 0.21 nm, which can be attributed to the (100) or (010) plane of the graphite structure. Moreover, the inserted fast Fourier transform (FFT) image indicates the hexagonal symmetry of the exfoliated graphite nanosheets (Figure 2i). Similarly, the mean nanosheets lengths $\langle L \rangle$ of *h*-BN, MoS_2, and WS_2 are extracted from bright field images in Figure 2b−d with magnitudes of about 120, 319, and 124 nm, respectively. And their most probable lengths L read from the centers of corresponding histograms are about 82 ± 5, 170 ± 5, and 76 ± 4 nm (Figure 2r−t), respectively. The HRTEM images show *d*-spacings of about 0.22 (Figure 2j), 0.28 (Figure 2k), and 0.27 (Figure 2l) nm, which correspond to the (100), (010), and (100) planes for *h*-BN, MoS_2, and WS_2 crystals, respectively. For exfoliated black P nanosheets, the average length $\langle L \rangle$ and most probable length L, extracted from bright field TEM images as in Figure 2e, are about 406 and 258 ± 3 nm, respectively (Figure 2u). The HRTEM image exhibits the lattice fringes of about 0.22 nm, which can be attributed to the (002) plane of the bulk crystal (Figure 2m). And the inset FFT reflects the symmetry of the stripped nanosheets. From TEM images in Figures 2f−h, the average lengths $\langle L \rangle$ and the most probable lengths L for hybrid frameworks MnDMS, Cu-P, and Cu-dca are about 67 and 57 ± 8, 91 and 58 ± 4, 149 and 100 ± 3 nm, respectively (Figure 2v−x). Like many MOFs and CPs, the nanosheets of MnDMS, Cu-P, and Cu-dca are very sensitive to the electron beam, which leads to rapid damage of lattice fringes within tens of seconds. Nevertheless, the HRTEM images were able to be captured after many trials. The *d*-spacings in Figure 2n−p are about 0.45, 0.21, and 0.24 nm, respectively. Which are associated with the (210), (201), and (044) planes for MnDMS, Cu-P, and Cu-dca crystal structures, respectively. Both the lattice fringes and FFT images confirm that the obtained nanosheets maintain good crystallinity after sonication.

As TEM only can provide information about the lateral lengths of nanosheets, we further performed atomic force microscopy (AFM) to obtain the statistical data about thickness of exfoliated nanosheets for all eight 2D materials at the same scanning conditions. Specifically, the aforementioned suspensions were diluted to a lower concentration of 0.1 mg/mL by ethanol to minimize agglomeration, and then these suspensions were dipped on preheated Si wafers which were left standing until the complete evaporation of ethanol. Prior to AFM characterizations, we performed Raman spectra (Figures S1−8) to confirm the existence of 2D material nanosheets, which are consistent with the above TEM experiments. As seen in the surface topographic images in Figure 3a−h, the exfoliated nanosheets with different color contrast show terraces at their edges. The corresponding height profiles of the nanosheets for all eight 2D materials display a number of steps which are approximate to the integral multiples of their monolayer thickness.[17] According to the heights of steps measured in these height profiles (Figures S1−8), the thickness of the monolayer for graphite, *h*-BN, MoS_2, WS_2, black P, MnDMS, Cu-P, and Cu-dca can be respectively determined as 0.8 (Figure S1),[18−20] 0.64 (Figure S2), 0.65,[21,22] 0.65,[23] 0.53,[24] 1.0,[13] 0.81,[11] and 1.1 nm, which are consistent with previous experimental and theoretical results. Considering the fact that these 2D materials have distinct monolayer thicknesses, we convert the measured AFM heights into number of layers (N). As shown in Figure 3i, the average

DOI: 10.1021/acs.chemmater.8b01082
Chem. Mater. 2018, 30, 8732−8738

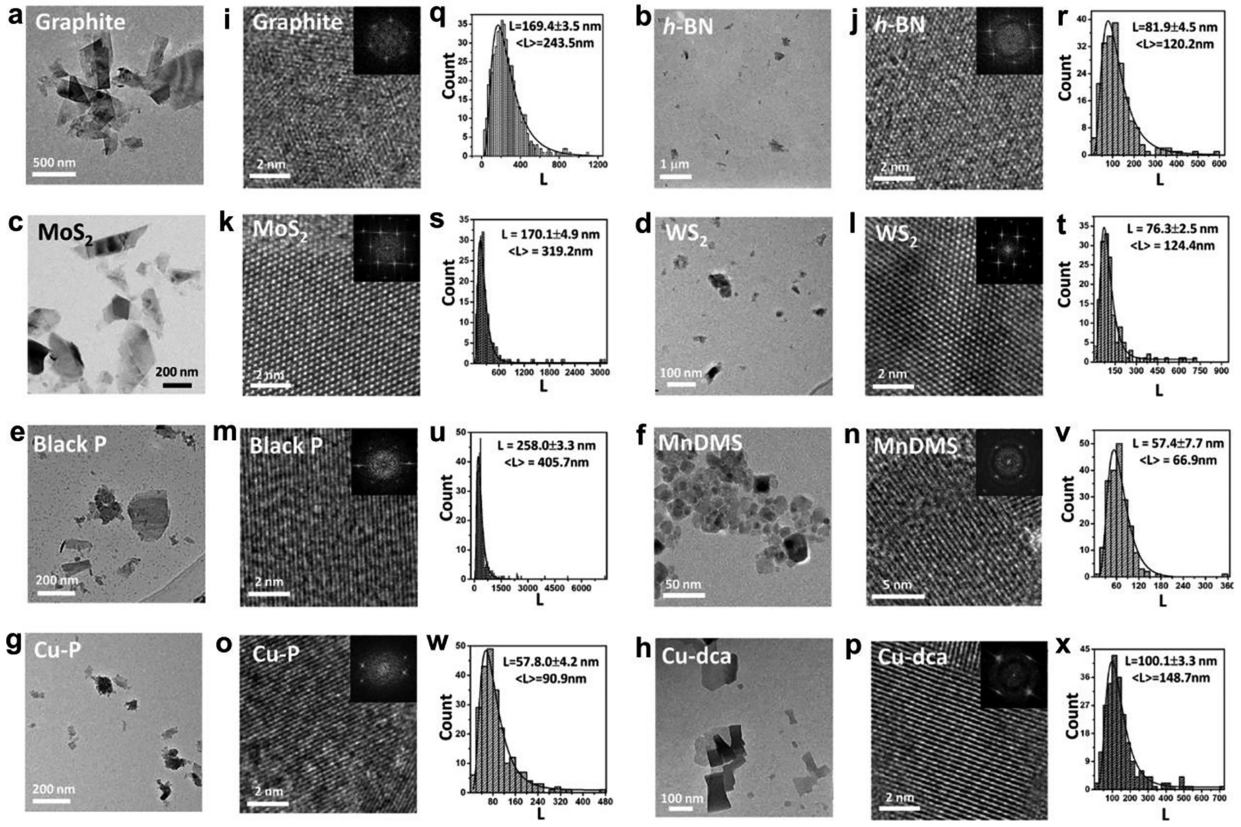

Figure 2. TEM characterizations of ethanol exfoliated nanosheets. The bright field morphologies of (a) graphite, (b) *h*-BN, (c) MoS_2, (d) WS_2, (e) black P, (f) MnDMS, (g) Cu-P, and (h) Cu-dca nanosheets. (i–p) The high resolution TEM (HRTEM) images and corresponding fast Fourier transforms (FFT) of these 2D materials. (q–x) Statistical distributions of nanosheets lateral size (L) for these 2D materials are extracted from the TEM images like those in parts (a)–(h), respectively. For each kind of 2D material, the statistical analysis was conducted from 160 to 400 nanosheets. The standard deviations of the mean values are listed in Table S4.

number of layers ($\langle N \rangle$) of graphite nanosheets is about 10 by statistically averaging 271 nanosheets. Meanwhile, the peak value of thickness (N) from the log-normal distribution fitting, which can reflect the most likely thickness of exfoliated nanosheets during the sonication, is about 5. Similarly, the distributions of nanosheets lengths (Figure 3q) also give the respective average and most probable length values ($\langle L \rangle$ and L) of about 245 and 210 ± 3 nm, which are in good agreement with the values of 244 and 169 ± 4 nm measured by TEM. The lateral sizes measured via AFM are slightly larger than those measured via TEM probably due to the tip broadening and pixilation effects of the AFM test. The most probable dimensional values of exfoliated nanosheets extracted from the corresponding statistical distributions for all eight 2D materials are presented in Figure 3. To more precisely reflect the exfoliation statistics, we use the most probable lengths (L) and thicknesses (N) in the following discussion. For example, the N and L of exfoliated black P and Cu-dca nanosheets are respectively about 39 ± 2 layers and 347 ± 1 nm (Figures 3m,u) and 26 ± 1 layers and 138 ± 2 nm (Figures 3p,x).

To evaluate the ease level of exfoliation from liquid-assisted sonication, both L and N need to be taken into accounted: large L and small N indicate easy exfoliation while small L and large N mean a difficult process. In this regard, using the L/N ratio will be more meaningful, and its magnitude scales with the exfoliation effectivity of 2D materials. For example, the L/N ratio of graphite is approximately 6.6 times larger than that of Cu-dca (Table S1), which suggests graphite bulks can be more easily cleaved to nanosheets than Cu-dca crystals under the same exfoliation conditions. Indeed, our attempts to Scotch-tape single crystals of Cu-dca could barely give any nanosheets which is in marked contrast to the facile cleavage of graphite bulks using same method. For all eight studied 2D materials, the magnitudes of their L/N values indicate their ease levels of exfoliation in the following order: graphite (39.6) > *h*-BN (12.3) > MoS_2 (11.3) > WS_2 (10.2) > black P (8.7) > MnDMS (7.5) > Cu-dca (5.2) > Cu-P (3.8).

We now examine the atomic bonding interactions and associated molecular mechanics to understand the underlying origins of the different exfoliation ease levels of 2D materials. As the interlayer bonding strength directly correlates the shear strength along the layer, stronger out-of-plane bonding strength would lead to more difficult separation of layers (Figure 4a). Specifically, stripping 2D layers bound via hydrogen bonding or electrostatic forces would be more difficult than peeling the layers interacting by van der Waals forces. On the other hand, the in-plane bonding strength also strongly influences the cleavage, as it reveals the firmness of the interlayer structure for resisting cracking to maintain the wide lateral size of nanosheets. In this respect, stronger in-plane bonding strength would give rise to larger lateral dimensions of the exfoliated nanosheets (Figure 4a). Considering both factors, the bonding strength contrast between in-plane and out-of-plane of 2D materials will be more meaningful for evaluating their ease levels of exfoliation.

DOI: 10.1021/acs.chemmater.8b01082
Chem. Mater. 2018, 30, 8732–8738

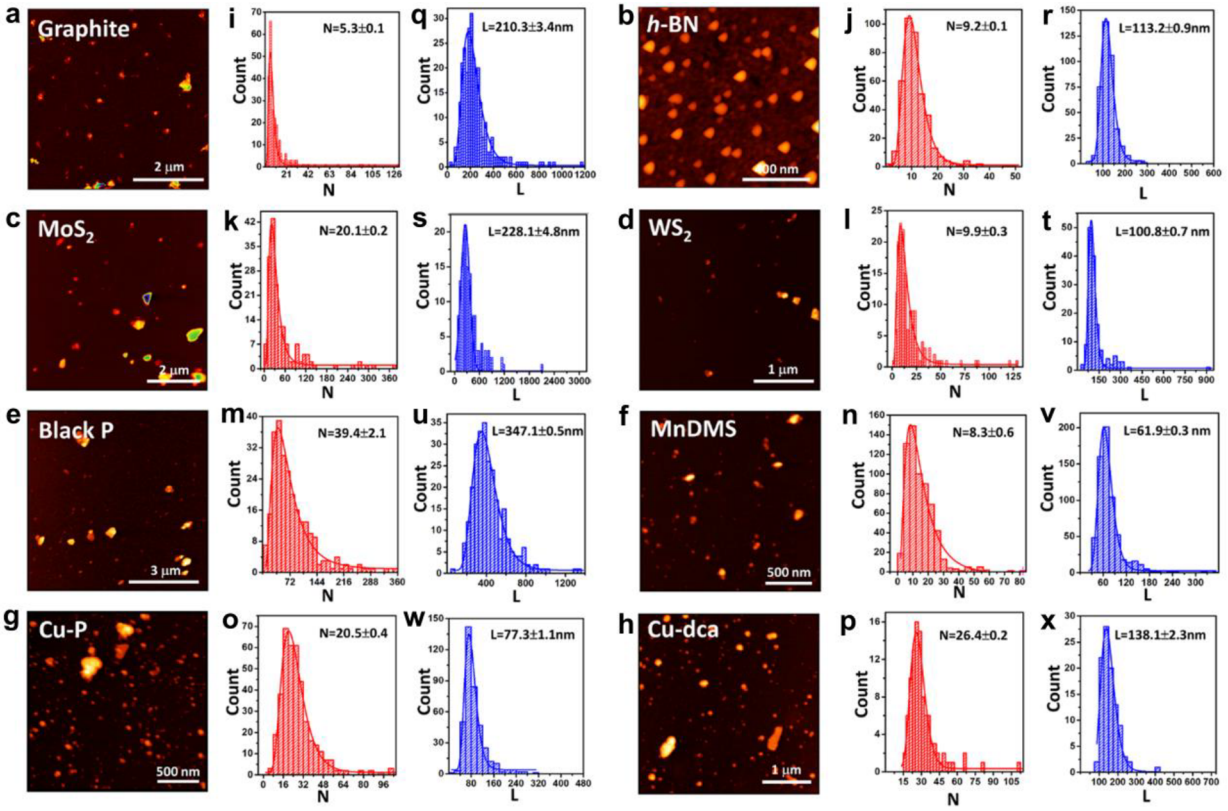

Figure 3. Wide field AFM topographies of ethanol exfoliated nanosheets of (a) graphite, (b) h-BN, (c) MoS_2, (d) WS_2, (e) black P, (f) MnDMS, (g) Cu-P, and (h) Cu-dca. The in-situ dimensional statistics of thicknesses (N) and lateral sizes (L) for exfoliated graphite (i, q), h-BN (j, r), MoS_2 (k, s), WS_2 (l, t), black P (m, u), MnDMS (n, v), Cu-P (o, w), and Cu-dca nanosheets (p, x). For each kind of 2D material, the statistical analysis was conducted from 160 to 300 nanosheets. Note: N is the thickness of nanosheets in terms of layer number.

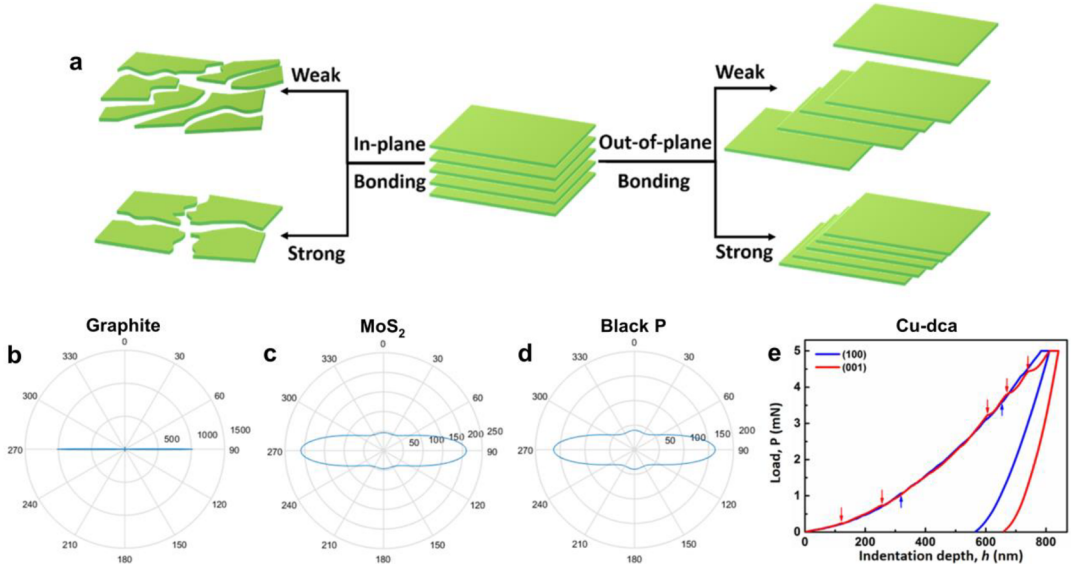

Figure 4. (a) Schematically illustrated influences of in-plane and out-of-plane bonding strengths in the exfoliation process. 2D polar plots of Young's modulus E (ref 25) projected normal to (100) plane for (b) graphite (ref 26), (c) MoS_2 (ref 27), and (d) black P (refs 24, 28, and 29). 0 and 90° are respectively along the out-of-plane and in-plane directions, corresponding to the c- and b-axes for graphite and MoS_2 and b and c-axes for black P. (e) Load-indentation depth (P–h) curves normal to the (100) and (001) planes of single crystals of $(TPrA)Cu(NO_3)(dca)_2$, which correspond to the out-of-plane and in-plane directions, respectively.

As the bonding forces can be directly reflected through the elastic modulus of materials which can be facilely obtained from routine mechanical experiments,[30,31] it is reasonable to use the ratio of in-plane/out-of-plane elastic modulus as an index ($A_{In/Out} = E_{In\text{-}plane}/E_{Out\text{-}of\text{-}plane}$) to quantify the exfoliation ease levels of 2D materials. As shown in the 2D polar plots of the elastic modulus in Figure 4b, the $E_{In\text{-}plane}$ and $E_{Out\text{-}of\text{-}plane}$ of the most exfoliatable graphites are 1025.2 and 36.1 GPa, which

DOI: 10.1021/acs.chemmater.8b01082
Chem. Mater. 2018, 30, 8732–8738

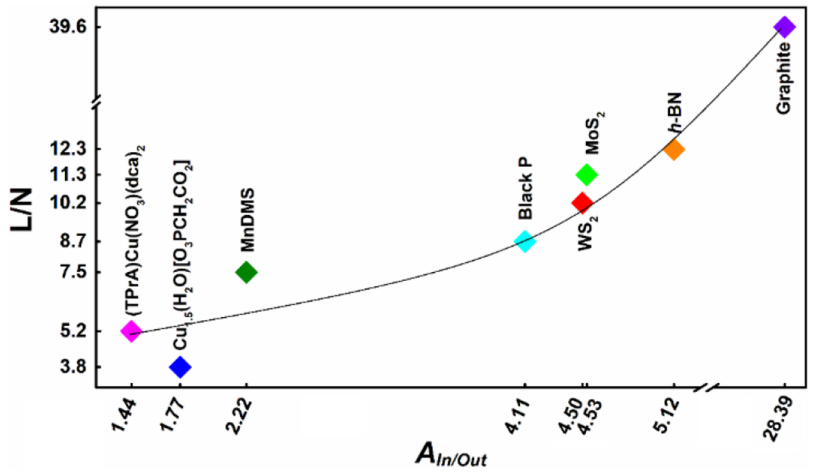

Figure 5. L/N ratio of exfoliated nanosheets for eight different 2D materials in dependence of their $A_{In/Out}$ index. Both L and N are the most probable values extracted from corresponding AFM statistics (Figure 3) via the log-normal fitting. The $A_{In/Out}$ values and the L/N ratios of these eight materials are listed in Table S1.

gives rise to a very large $A_{In/Out}$ ratio of 28.39/1. However, the 2D polar plots of elastic modulus for the moderately exfoliatable *h*-BN,[32] MoS_2, WS_2,[33] and black P (Figure 4c,d, Table S1) show smaller $A_{In/Out}$ ratios of 5.12/1, 4.53/1, 4.50/1, and 4.11/1, respectively. Though all the above five 2D materials are van der Waals crystals, their different in-plane bonding strengths give them distinct $A_{In/Out}$ ratios. For the weakly exfoliatable coordination polymers MnDMS[11] and Cu-P,[9] the interlayer interactions are respectively van der Waals forces and relatively stronger hydrogen-bonding, which lead to a lower $A_{In/Out}$ ratio of Cu-P (1.77) than that of MnDMS (2.22). The $A_{In/Out}$ ratio of the least exfoliatable Cu-dca, obtained via nanoindentation experiments (Figure 4e), is further lowered to 1.434/1, which arises from its corrugated $Cu(NO_3)(dca)_2^-$ layers, strong interlayer electrostatic interactions, and the dense packing structural fashion.

Having both L/N ratios and $A_{In/Out}$ indexes, we now can plot their relationship to fully quantify the ease levels of exfoliation for all eight 2D materials. As displayed in Figure 5, the L/N ratios extracted from Figure 3 for these eight materials are proportional to their $A_{In/Out}$ indexes, which reveals that 2D materials with large mechanical anisotropy tend to be more exfoliatable. Specifically, the $A_{In/Out}$ values of coordination polymers Cu-P[9] and MnDMS[11] are respectively about 23% and 54% larger than the lowest value of analogous Cu-dca (Table S1), which correspond to 27% lower and 44% higher L/N ratios of the exfoliated nanosheets (Figure 3p,x). Compared with these three coordination polymers, the several times to an-order-of magnitude higher $A_{In/Out}$ values of the other five van der Waals 2D materials naturally result in significantly larger L/N ratios as verified by our sonication experiments (Figure 3). For instance, the highest L/N ratio of about 39.6 for graphite nanosheets indicates its easiest exfoliation level among all eight materials, which is essentially attributed to its largest $A_{In/Out}$ of 28.39 (Figure 4b). Note that the slight deviation of Cu-P from the $A_{In/Out}$ vs L/N plot is very likely due to the affinity and restacking of the exfoliated nanosheets via H-bonding attractions (Figures 2g and 3g,o). In addition, we plotted the ratio of average lateral lengths and thicknesses ($\langle L\rangle/\langle N\rangle$) in dependence of $A_{In/Out}$ as demonstrated in Figure S9, which shows a trend similar to that in Figure 5, further confirming the robust relationship between exfoliatability and mechanical anisotropy.

CONCLUSIONS

In summary, we have systematically studied the mechanical exfoliation of eight prototypical 2D materials with different molecular bonding features including van der Waals forces, hydrogen bonding, and electrostatic interactions at same experimental conditions. Our statistical TEM and AFM analyses of these 2D materials demonstrate that the ratio of lateral size and number of layers (L/N) of the exfoliated nanosheets can approximate their ease levels of exfoliation. In addition, we reveal that the ease levels for exfoliating these 2D materials into thin nanosheets are proportional to the magnitude of their mechanical anisotropies between in-plane and out-of-plane. More importantly, we define an experimentally available index, $A_{In/Out}$ ($= E_{In\text{-}plane}/E_{Out\text{-}of\text{-}plane}$), to quantify the ease level of exfoliation of 2D materials. Considering the soaring demand for scaling down many new emerged 2D materials into thin nanosheets,[34,35] such a simple index could be instructive for selecting an appropriate exfoliation methodology.

ASSOCIATED CONTENT

Supporting Information

The Supporting Information is available free of charge on the ACS Publications website at DOI: 10.1021/acs.chemmater.8b01082.

Experimental details (EA, TGA, FT-IR, single-crystal X-ray diffraction, TEM, AFM, and nanoindentation), Raman and AFM results of exfoliated nanosheets of each 2D material, elastic moduli of 2D materials and corresponding L/N and $\langle L\rangle/\langle N\rangle$ ratios, $\langle L\rangle/\langle N\rangle$ ratio vs $A_{In/Out}$ plots (both $\langle L\rangle$ and $\langle N\rangle$ are the average values), and characterizations of the newly synthesized $(TPrA)Cu(NO_3)(dca)_2$ (PDF)

Crystallographic information (CIF)

AUTHOR INFORMATION

Corresponding Authors

*Wei Li. E-mail: wl276@hust.edu.cn and wl276@nankai.edu.cn.

DOI: 10.1021/acs.chemmater.8b01082
Chem. Mater. 2018, 30, 8732−8738

*Peixiang Lu. E-mail: lupeixiang@hust.edu.cn..

ORCID

Wei Li: 0000-0002-5277-6850

Xiaodong Li: 0000-0002-2290-1198

Notes

The authors declare no competing financial interest.

■ ACKNOWLEDGMENTS

Financial support from the National Natural Science Foundation of China (No. 21571072) is gratefully acknowledged.

■ REFERENCES

(1) Novoselov, K. S.; Geim, A. K.; Morozov, S. V.; Jiang, D.; Zhang, Y.; Dubonus, S. V.; Grigorieva, I. V.; Firsov, A. A. Electric Field Effect in Atomically Thin Carbon Films. *Science* **2004**, *306*, 666−669.

(2) Liu, W.-W.; Xing, J.; Zhao, J.-X.; Wen, X.-L.; Wang, K.; Lu, P.-X.; Xiong, Q.-H. Giant Two-Photon Absorption and Its Saturation in 2D Organic-Inorganic Perovskite. *Adv. Opt. Mater.* **2017**, *5*, 1601045.

(3) Mannix, A. J.; Kiraly, B.; Hersam, M. C.; Guisinger, N. P. Synthesis and Chemistry of Elemental 2D Materials. *Nat. Rev. Chem.* **2017**, *1*, 0014.

(4) Junggeburth, S. C.; Diehl, L.; Werner, S.; Duppel, V.; Sigle, W.; Lotsch, B. V. Ultrathin 2D Coordination Polymer Nanosheets by Surfactant-Mediated Synthesis. *J. Am. Chem. Soc.* **2013**, *135*, 6157−6164.

(5) Sakamoto, R.; Takada, K.; Sun, X.; Pal, T.; Tsukamoto, T.; Phua, E. J. H.; Rapakousiou, A.; Hoshiko, K.; Nishihara, H. The Coordination Nanosheet (CONASH). *Coord. Chem. Rev.* **2016**, *320-321*, 118−128.

(6) Miyamoto, N.; Nakato, T. Liquid Crystalline Nanosheet Colloids with Controlled Particle Size Obtained by Exfoliating Single Crystal of Layered Niobate $K_4Nb_6O_{17}$. *J. Phys. Chem. B* **2004**, *108*, 6152−6159.

(7) Nicolosi, V.; Chhowalla, M.; Kanatzidis, M. G.; Strano, M. S.; Coleman, J. N. Liquid Exfoliation of Layered Materials. *Science* **2013**, *340*, 1226419.

(8) Tongay, S.; Zhou, J.; Ataca, C.; Lo, K.; Matthews, T. S.; Li, J.-B.; Grossman, J. C.; Wu, J.-Q. Thermally Driven Crossover from Indirect toward Direct Bandgap in 2D Semiconductors: $MoSe_2$ versus MoS_2. *Nano Lett.* **2012**, *12*, 5576−5580.

(9) Tan, J. C.; Merrill, C. A.; Orton, J. B.; Cheetham, A. K. Anisotropic Mechanical Properties of Polymorphic Hybrid Inorganic-Organic Framework Materials with Different Dimensionalities. *Acta Mater.* **2009**, *57*, 3481−3496.

(10) Wu, Q.; Sjåstad, A. O.; Vistad, O. B.; Knudsen, K. D.; Roots, J.; Pedersen, J. S.; Norby, P. Characterization of Exfoliated Layered Double Hydroxide (LDH, Mg/Al = 3) Nanosheets at High Concentrations in Formamide. *J. Mater. Chem.* **2007**, *17*, 965−975.

(11) Tan, J. C.; Saines, P. J.; Bithell, E. G.; Cheetham, A. K. Hybrid Nanosheets of an Inorganic-Organic Framework Material: Facile Synthesis, Structure, and Elastic Properties. *ACS Nano* **2012**, *6*, 615−621.

(12) Dou, L.; Wong, A. B.; Yu, Y.; Lai, M. L.; Kornienko, N.; Eaton, S. W.; Fu, A.; Bischak, C. G.; Ma, J.; Ding, T.; Ginsberg, N. S.; Wang, L.-W.; Alivisatos, A. P.; Yang, P. Atomically Thin Two-Dimensional Organic-Inorganic Hybrid Perovskite. *Science* **2015**, *349*, 1518−1521.

(13) Peng, Y.; Li, Y.; Ban, Y.; Jin, H.; Jiao, W.; Liu, X.; Yang, W. Metal-Organic Framework Nanosheets As Building Blocks for Molecular Sieving Membranes. *Science* **2014**, *346*, 1356−1359.

(14) Liscio, A.; Kouroupis-Agalou, K.; Betriu, X. D.; Kovtun, A.; Treossi, E.; Pugno, N. M.; De Luca, G.; Giorgini, L.; Palermo, V. Evolution of the size and shape of 2D nanosheets during ultrasonic fragmentation. *2D Mater.* **2017**, *4*, 025017.

(15) Kouroupis-Agalou, K.; Liscio, A.; Treossi, E.; Ortolani, L.; Morandi, V.; Pugno, N. M.; Palermo, V. Fragmentation and Exfoliation of 2-Dimensional Materials: a Statistical Approach. *Nanoscale* **2014**, *6*, 5926−5933.

(16) Goncalves, G.; Vila, A.; Bdikin, L.; de Andres, A.; Emami, N.; Ferreira, R. A. S.; Carlos, L. D.; Gracio, J.; Marques, P. A. A. P. Breakdown into Nanoscale of Graphene Oxide: Confined Hot Spot Atomic Reduction and Fragmentation. *Sci. Rep.* **2015**, *4*, 6735.

(17) Backes, C.; Szydlowska, B. M.; Harvey, A.; Yuan, S.; Vega-Mayoral, V.; Davies, B. R.; Zhao, P.; Hanlon, D.; Santos, E. J. G.; Katsnelson, M. I.; Blau, W. J.; Gadermaier, C.; Coleman, J. N. Production of Highly Monolayer Enriched Dispersions of Liquid-Exfoliated Nanosheets by Liquid Cascade Centrifugation. *ACS Nano* **2016**, *10*, 1589−1601.

(18) Ishigami, M.; Chen, J. H.; Cullen, W. G.; Fuhrer, M. S.; Williams, E. D. Atomic Structure of Graphene on SiO_2. *Nano Lett.* **2007**, *7*, 1643−1648.

(19) Nemes-Incze, P.; Osváth, Z.; Kamarás, K.; Biró, L. P. Anomalies in Thickness Measurements of Graphene and Few Layer Graphite Crystals by Tapping Mode Atomic Force Microscopy. *Carbon* **2008**, *46*, 1435−1442.

(20) Shearer, C. J.; Slattery, A. D.; Stapleton, A. J.; Shapter, J. G.; Gibson, C. T. Accurate Thickness Measurement of Graphene. *Nanotechnology* **2016**, *27*, 125704.

(21) Mattheiss, L. F. Band Structures of Transition-Metal-Dichalcogenide Layer Compounds. *Phys. Rev. B* **1973**, *8*, 3719−3740.

(22) Li, H.; Wu, J.; Yin, Z.; Zhang, H. Preparation and Applications of Mechanically Exfoliated Single-Layer and Multilayer MoS_2 and WS_2 Nanosheets. *Acc. Chem. Res.* **2014**, *47*, 1067−1075.

(23) Mccreary, K. M.; Hanbicki, A. T.; Singh, S.; Kawakami, R. K.; Jernigan, G. G.; Ishigami, M.; Ng, A.; Brintlinger, T. H.; Stroud, R. M.; Jonker, B. T. The Effect of Preparation Conditions on Raman and Photoluminescence of Monolayer WS_2. *Sci. Rep.* **2016**, *6*, 35154.

(24) Wang, Z.; Feng, P. X. L. Design of Black Phosphorus 2D Nanomechanical Resonators by Exploiting the Intrinsic Mechanical Anisotropy. *2D Mater.* **2015**, *2*, 021001.

(25) Dong, L.-Y.; Sun, S.-J.; Deng, Z.-Y.; Li, W.; Wei, F.-X.; Qi, Y.-J.; Li, Y.-C.; Li, X.-D.; Lu, P.-X.; Ramamurty, U. Elastic Properties and Thermal Expansion of Lead-Free Halide Perovskite $Cs_2AgBiBr_6$. *Comput. Mater. Sci.* **2018**, *141*, 49−58.

(26) Blakslee, O. L.; Proctor, D. G.; Seldin, E. J.; Spence, G. B.; Weng, T. Elastic Constants of Compression-Annealed Pyrolytic Graphite. *J. Appl. Phys.* **1970**, *41*, 3373−3382.

(27) Feldman, J. Elastic Constants of 2H-MoS_2 and 2H-$NbSe_2$ Extracted from Measured Dispersion Curves and Linear Compressibilities. *J. Phys. Chem. Solids* **1976**, *37*, 1141−1144.

(28) Wei, Q.; Peng, X. Superior Mechanical Flexibility of Phosphorene and Few-Layer Black Phosphorus. *Appl. Phys. Lett.* **2014**, *104*, 251915.

(29) Appalakondaiah, S.; Vaitheeswaran, G.; Lebegue, S.; Christensen, N. E.; Svane, A. Effect of van der Waals Interactions on the Structural and Elastic Properties of Black Phosphorus. *Phys. Rev. B: Condens. Matter Mater. Phys.* **2012**, *86*, 035105.

(30) Varughese, S.; Kiran, M. S. R. N.; Ramamurty, U.; Desiraju, G. R. Nanoindentation in Crystal Engineering: Quantifying Mechanical Properties of Molecular Crystals. *Angew. Chem., Int. Ed.* **2013**, *52*, 2701−2712.

(31) Gui, D.; Ji, L.; Muhammad, A.; Li, W.; Cai, W.; Li, Y.; Li, X.; Wu, X.; Lu, P. Jahn-Teller Effect on Framework Flexibility of Hybrid Organic-Inorganic Perovskites. *J. Phys. Chem. Lett.* **2018**, *9*, 751−755.

(32) Peng, Q.; Ji, W.; De, S. Mechanical Properties of the Hexagonal Boron Nitride Monolayer: Ab Initio Study. *Comput. Mater. Sci.* **2012**, *56*, 11−17.

(33) Feng, L. P.; Wang, Z. Q.; Liu, Z. T. First-Principles Calculations on Mechanical and Elastic Properties of 2H- and 3R-WS_2 under Pressure. *Solid State Commun.* **2014**, *187*, 43−47.

(34) Mounet, N.; Gibertini, M.; Schwaller, P.; Campi, D.; Merkys, A.; Marrazzo, A.; Sohier, T.; Castelli, I. E.; Cepellotti, A.; Pizzi, G.; Marzari, N. Two-Dimensional Materials from High-Throughput Computational Exfoliation of Experimentally Known Compounds. *Nat. Nanotechnol.* **2018**, *13*, 246−252.

DOI: 10.1021/acs.chemmater.8b01082
Chem. Mater. 2018, 30, 8732−8738

(35) Feng, G.; Qin, Y.; Ran, C.; Ji, L.; Dong, L.; Li, W. Structural Evolution and Photoluminescence Properties of a 2D Hybrid Perovskite under Pressure. *APL Mater.* **2018**, *6*, 114201.

DOI: 10.1021/acs.chemmater.8b01082
Chem. Mater. 2018, 30, 8732−8738